International Journal of Heat and Mass Transfer 52 (2009) 451–459

Contents lists available at ScienceDirect

International Journal of Heat and Mass Transfer

journal homepage: www.elsevier.com/locate/ijhmt

Interfacial heat transfer coefficients and solidification of an aluminum alloy in a rotary continuous caster

Noé Cheung [a], Newton S. Santos [b], José M.V. Quaresma [c], George S. Dulikravich [d], Amauri Garcia [a,*]

[a] Department of Materials Engineering, University of Campinas, UNICAMP P.O. Box 6122, 13083–970 Campinas, SP, Brazil.
[b] Alubar Metals, Belém, PA, Brazil
[c] Federal University of Pará, UFPA, Belém, PA, Brazil
[d] Department of Mechanical and Materials Engineering, Florida International University, Miami, Fl, USA

ARTICLE INFO

Article history:
Received 9 April 2007
Received in revised form 10 April 2008
Available online 20 August 2008

Keywords:
Rotary continuous casting
Aluminum alloy
Properzi process
Solidification numerical modeling

ABSTRACT

The present study describes the development of an experimental set-up representing the metal/mold system of a rotary continuous caster as part of a methodology, which connected to a numerical heat transfer model permits to determine transient metal/mold heat transfer coefficients, *h*, during solidification. By using this approach the variation of *h* along the different mold walls and the metal surface has been investigated by a method based on numerically calculated/experimental fit of thermal profiles (IHCP). The results have shown that the used methodology permits the characterization of *h* and may be used in the simulation of solidification in industrial processes.

1. Introduction

In recent decades, a dramatic growth of the continuous casting technology has been realized for both ferrous and non-ferrous metals production. The principal advantages of continuous casting are a substantial improve in yield, a more uniform product, energy savings, and higher productivity [1].

The principal continuous casting process for light metals is the direct-chill process. It can directly prepare billets for extrusion, blocks for rolling and sheet for fabrication, thus eliminating intermediate mechanical working processes by casting near-net shapes [1]. Twin-roll casting is a proven technology for economical production of thin aluminum sheet directly from the melt. The advantages of this casting technique are numerous – reduced capital costs, energy consumption, operating costs and scrap rate compared with a conventional direct chill process. Despite its large potential, twin roll casting is still a difficult process to control [2,3]. Rod and bar are continuously cast on wheel and band machines, such as the rotary continuous caster (Properzi process). This process involves casting between the circumference of a large copper rimmed wheel containing the mold configuration and a steel band (Fig. 1). The casting wheel rotates on its axis driven by a variable speed motor. The molten charge is held in place against a drum by a steel band, and the metal solidifies in the gap as the wheel and the band rotate. The liquid metal is quickly solidified by the action of externally mounted and controlled water sprays placed around the external periphery of the mold. The production rate depends on the length of the solidification arc, which is proportional to the casting wheel diameter [1,4].

Modeling of casting solidification can provide a method for improving casting yields. An accurate casting solidification model could be used to predict microstructure and to control the process based on thermal and operational parameters. The idea of using simulation to optimize a continuous caster is not just a theoretical concept and its practicality has already been demonstrated [5,6]. Numerical approaches which are based on the interaction of finite difference heat transfer solidification models with neural network based algorithms, knowledge bases of metallurgical constraints, and heuristic search techniques have been successfully applied in the simulation of continuous casting [7–9].

Casting simulation requires high quality information concerning thermophysical properties and operational thermal variables [10,11]. For the purpose of accurate mathematical modeling of solidification in the continuous casting process, it is essential that correct boundary conditions be established along the caster machine during casting operations. Heat transfer at the metal/cooling interface is one of these boundary conditions, which is of central importance when considering the magnitude of heat transfer during the stages of solidification in the mold, spray zones or natural cooling. Many investigations concerning the heat transfer coefficient between metal and mold in casting systems have been carried out, and pointed out the importance of the development of appropriate tools to predict the heat transfer coefficient, *h*. Most of

* Corresponding author. Tel.: +55 19 3521 3320; fax: +55 19 3289 3722.
E-mail address: amaurig@fem.unicamp.br (A. Garcia).

0017-9310/$ - see front matter © 2008 Elsevier Ltd. All rights reserved.
doi:10.1016/j.ijheatmasstransfer.2008.07.003

Nomenclature

A	cross-section area [m^2]
a	constant which depends on solidification conditions [dimensionless]
c	specific heat [J/kg.K]
c'	pseudo-specific heat [J/kg.K]
f_s	local solid fraction [%]
h	transient interfacial heat transfer coefficient [$W/m^2.K$]
$h_{lateral}$, h_{up}, h_{bottom}	heat transfer coefficients acting at the metal/mold interfaces [$W/m^2.K$]
h_{water}	heat transfer coefficients acting at the mold/ cooling water interfaces [$W/m^2.K$]
i	element position according to 'x' and 'y' axes [dimensionless]
L	latent heat [J/kg]
k_0	partition coefficient
K	thermal conductivity [W/m.K]
K_{eq}	equivalent thermal conductivity [W/m.K]
m	constant which depends on solidification conditions [dimensionless]
$\dot{q}$	rate of energy generation [W/m^3]
T	temperature [K]
T_{est}	estimated temperature [K]
T_{exp}	experimentally measured temperature [K]
T_f	melting temperature [K]
T_{Liq}	liquidus temperature [K]
T_{metal}	ingot temperature [K]
T_{mold}	mold temperature [K]
T_{mw}	temperature at the mold wall [K]
T_∞	coolant temperature [K]
t	time [s]
x_i	rectangular coordinate in horizontal or vertical directions [m]
x_{mew}	position at the ingot wall [m]
x_{mw}	position at the mold wall [m]

Greek Symbols

Δt	time interval [s]
ρ	density [kg/m^3]
ϕ	sensitivity coefficient [m^2/W]

Subscripts

S	solid
L	liquid
M	mushy

the methods of calculation of h existing in the literature are based on temperature histories at points of the casting or mold together with mathematical models of heat transfer during solidification. Among these methods, those based on the solution of the inverse heat conduction problem (IHCP) have been widely used in the quantification of the transient interfacial heat transfer [12–19].

There is a lack of consistent studies and experimental reports on the evolution of solidification in rotary continuous casters. The present study aims to contribute to the understanding of the role of the transient interfacial heat transfer coefficient at the different mold walls on the evolution of solidification of aluminum alloys in a Properzi machine. An experimental set-up representing the metal/mold system of an industrial rotary continuous caster was used connected to a numerical heat transfer model in order to permit transient metal/mold heat transfer coefficients to be determined along the four different metal/mold interfaces.

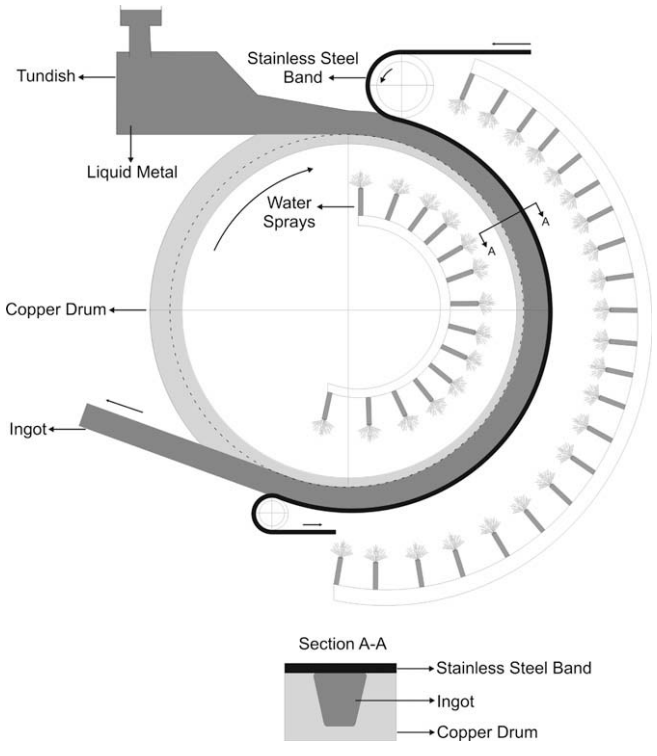

Fig. 1. Schematic of a rotary continuous caster.

2. Experimental procedure

The experimental simulator, schematically shown in Fig. 2, consists of a sector withdrawn from a Properzi wheel, which is chilled by common nozzles used in the industrial machine. The mold is made of copper and had its top covered by a stainless steel band which was extracted from the regular band that covers the industrial wheel. Insulating materials were placed in both ends of the mold and one of them was embedded with thermocouples placed into contact with the copper mold and with the aluminum alloy. The inner surface of the mold was mechanically polished using abrasive papers and no coatings had been applied. The mold and the spray system are supported by a bar, with the length of the wheel radius, which is able to rotate, representing several positions of the wheel, as shown in Fig. 2. In the present study, the support bar was kept displaced 5° from the vertical position, which is the configuration used for pouring the liquid metal in the industrial equipment. The photo of Fig. 3 shows the Properzi simulator in operation.

The alloy was melted in an electric resistance-type furnace until the molten metal reached a predetermined temperature. The mold was heated in a furnace and when the industrial wheel working temperature was achieved, the molten metal was poured into the casting chamber and at the same time the controlled water flow was initiated. The water flow was kept constant at about 40 L/min and controlled by a rotameter.

Fig. 4 shows the cross section of the mold with its dimensions and thermocouples positions. In order to obtain the experimental temperature profiles, iron–constantan thermocouples were placed in the mold and at different depths inside the casting in order to minimize their influence along solidification. Temperature measurements were collected at a rate of about two measurements per second by a computer-aided data logging system. After solidi-

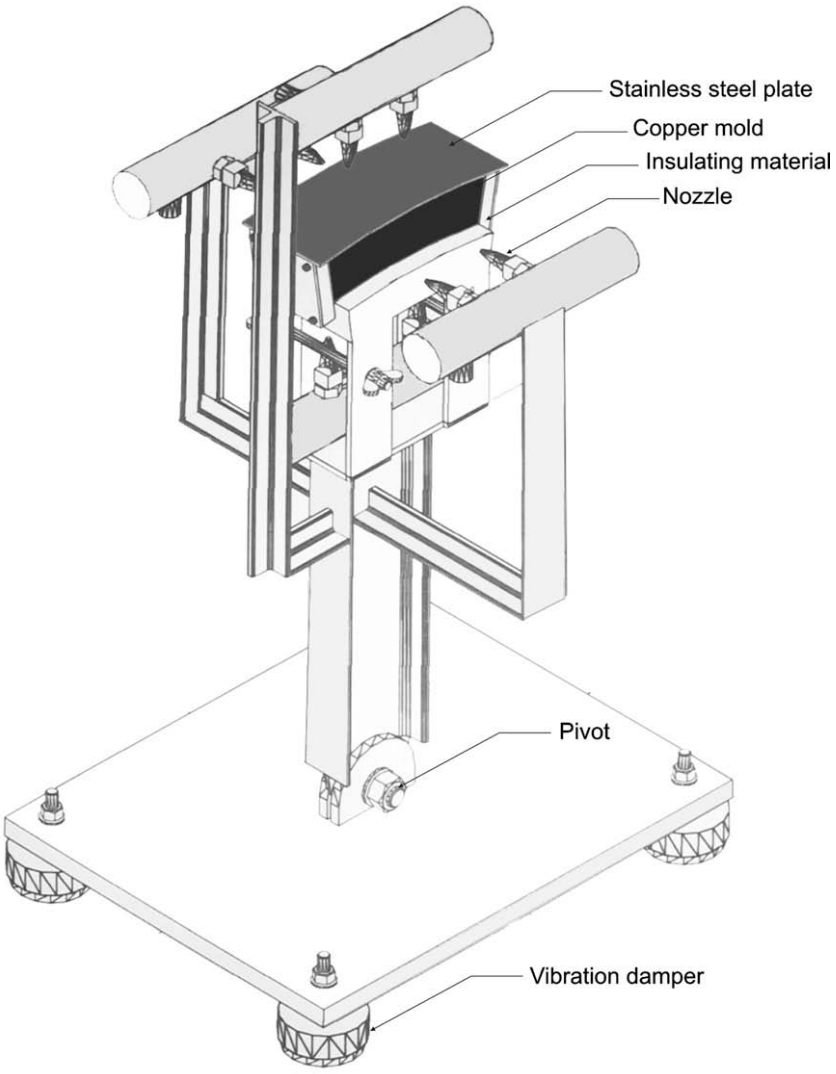

Fig. 2. Schematic representation of the experimental Properzi simulator.

Fig. 3. Properzi simulator in operation.

fied, the ingot was cross-sectioned to confirm the thermocouples positions.

A commercial 6101 aluminum alloy, used in Properzi casting machines to cast rods for the manufacturing of electric conductors, was chosen as the experimental material. Samples were analyzed by mass spectrometry and the chemical composition of such alloy is shown in Table 1.

3. Numerical model

Fig. 5 shows schematically the physical system to be modeled. The heat extracted from the simulator is a function of heat transfer coefficients acting at the metal/mold interfaces (h_{lateral}, h_{up}, h_{bottom}) and at the mold/cooling water interfaces (h_{water}). The mathematical formulation of heat transfer permitting the analysis of temperature evolution along solidification is based on the fundamental equation of heat conduction in its one dimensional form [20].

$$\rho c \frac{\partial T}{\partial t} = \frac{\partial}{\partial x_i}\left(K(x)\frac{\partial T}{\partial x_i}\right) + \dot{q} \tag{1}$$

where K, thermal conductivity [W/mK];
c, specific heat [J/kgK];
ρ, density [kg/m^3];
$\dot{q}$, rate of energy generation [W/ m^3];
T, temperature [K];
t, time [s] ;
x_i, rectangular coordinate in horizontal or vertical directions according to Fig. 5 [m].

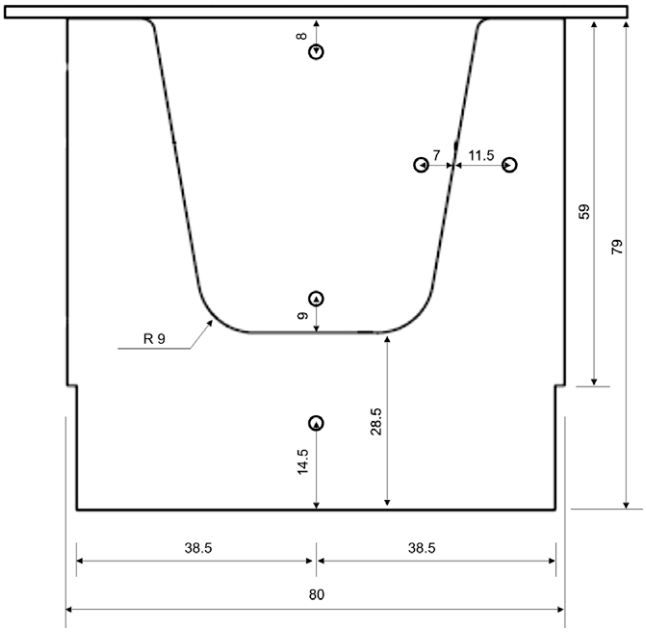

Fig. 4. Mold dimensions (mm) and thermocouples positions.

The release of latent heat between liquidus and solidus temperatures is expressed by $\dot{q}$:

$$\dot{q} = \rho L \frac{\delta f_S}{\delta t} \tag{2}$$

where L, latent heat [J/kg];

f_s, local solid fraction [%].

The fraction of solid in the mushy zone can be estimated by the Scheil equation, which assumes perfect mixing in the liquid and no solid diffusion. With liquidus and solidus lines having constant slopes, f_s is then expressed as:

$$f_s = 1 - \left(\frac{T_f - T}{T_f - T_{Liq}}\right)^{\frac{1}{k_0 - 1}} \tag{3}$$

where T_f, melt temperature [K];

T_{Liq}, liquidus temperature [K];

k_0, partition coefficient.

Eq. (3) is incorporated into the latent heat term (Eq. (2)) by differentiating the Scheil equation with respect to temperature. Hence, applying the chain rule of differentiation, we have:

$$\frac{\partial f_s}{\partial t} = \frac{1}{(k_0 - 1)(T_f - T_{liq})}\left(\frac{T_f - T}{T_f - T_{liq}}\right)^{\frac{2-k_0}{k_0 - 1}} \frac{\partial T}{\partial t} \tag{4}$$

Substituting Eq. (2) into Eq. (1) gives:

$$\rho c' \frac{\partial T}{\partial t} = \frac{\partial}{\partial x_i}\left(K(x_i)\frac{\partial T}{\partial x_i}\right) \tag{5}$$

where c' can be considered as a pseudo-specific heat capacity given by:

$$c' = c_M - L\frac{\partial f_s}{\partial T} \tag{6}$$

$$c_M = (1 - f_s)c_L + f_s c_S \tag{7}$$

where the subscripts S, L and M refer to solid, liquid and mushy, respectively.

Table 1
Chemical composition of the 6101 aluminum alloy [wt.%]

Si	Fe	Ti	Mn	Mg	V	Ni	B	Other	Al
0.550	0.240	0.010	0.005	0.550	0.002	0.003	0.002	0.017	98.62

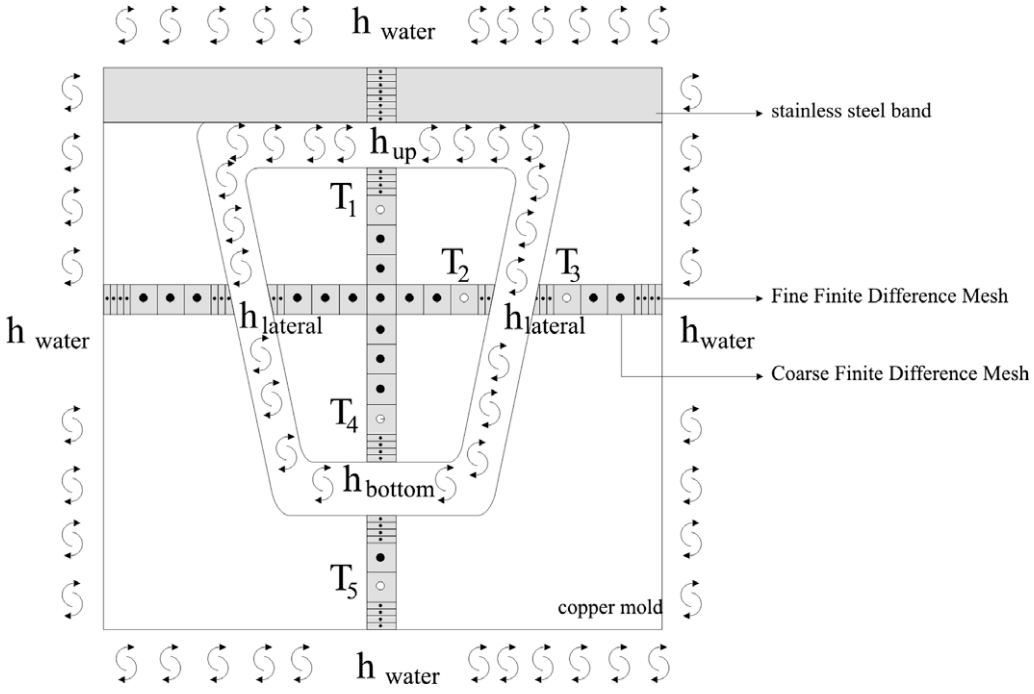

Fig. 5. Schematic representation of the physical problem.

The other properties such as thermal conductivity and density in the mushy zone are described similarly as the specific heat in Eq. (7):

$$K_M = (1 - f_s)K_L + f_s K_S \tag{8}$$

$$\rho_M = (1 - f_s)\rho_L + f_s \rho_S \tag{9}$$

A finite difference form of Eq. (5) is obtained for the time-dependent temperature distribution at discrete grid points:

$$(\rho.c')_i \frac{T_i^{n+1} - T_i^n}{\Delta t} = \frac{1}{\Delta x}\left(K_{i+1/2}\frac{T_{i+1}^n - T_i^n}{\Delta x} - K_{i-1/2}\frac{T_i^n - T_{i-1}^n}{\Delta x}\right) \tag{10}$$

where 'n' and '$n+1$' refer to temperatures before and after the incremental time interval Δt, 'i' is the element position according to 'x' and 'y' axes.

$K_{i+1/2}$ and $K_{i-1/2}$ are given by:

$$K_{i+1/2} = \frac{K_{i+1} + K_i}{2} \tag{11}$$

$$K_{i-1/2} = \frac{K_i + K_{i-1}}{2} \tag{12}$$

For dilute alloys which can be assumed to freeze congruently and for the remaining liquid of eutectic composition, the latent heat released during solidification can be taken into account by a device, which considers a temperature accumulation factor λ [21], given by

$$\lambda = \frac{L}{c_L} \tag{13}$$

The quantity λ must be regarded as a temperature change in the material, in the course of which an amount of specific heat equal to the latent heat would be evolved. When during the calculations the temperature of a network point falls below the melting temperature, T_f, the number of degrees by which it does so is subtracted from the indicated temperature, thus restoring the temperature of the point to T_f. The excess degrees that have been subtracted are being accumulated during the procedure and when it reaches the quantity λ the temperature of the network point is allowed to fall again. In physical terms, this calculation procedure disregards the heat source in Eq. (1) and $c' = c_L$ must be assumed in Eq. (10).

As shown in Figs. 4 and 5, the thermocouples were inserted inside the metal, positioned close to the centre of each metal/mold surface, i.e., metal/steel band (T_1), metal/mold lateral (T_2) and metal/mold bottom (T_4) as well as inside the mold along the heat flow path (T_3 and T_5). Due to such thermocouple distribution, two one-dimensional meshes with different sizes have been adopted to characterize heat flow in the numerical calculations, as depicted qualitatively in Fig. 5. The developed model uses different grid sizes: for the region near the interfaces, i. e., metal/mold and mold/coolant fluid, a refined grid was used whilst in remaining regions a coarser grid was applied. The connection between these meshes demands a heat balance in the fine/coarse meshes boundary, as indicated by Fig. 6.

$$T_c^{n+1} = \frac{\Delta t}{(\rho c)_c \Delta x_c}\left[\frac{K(T_{c+1}^n - T_c^n)}{\Delta x_c} + 2\frac{K(T_{fe}^n - T_c^n)}{\Delta x_{fe} + \Delta x_c}\right] + T_c^n \tag{14}$$

$$T_{fe}^{n+1} = \frac{\Delta t}{(\rho c)_{fe} \Delta x_{fe}}\left[\frac{K(T_{fe-1}^n - T_{fe}^n)}{\Delta x_{fe}} + 2\frac{K(T_c^n - T_{fe}^n)}{\Delta x_{fe} + \Delta x_c}\right] + T_{fe}^n \tag{15}$$

The different metal/mold and mold/cooling water interfaces are characterized by boundary conditions represented by heat transfer coefficients 'h' [W.m^{-2}.K^{-1}] in each face (h_{up}, h_{bottom}, h_{side}, h_{water}). The following equation is obtained by applying thermal balances at such interfaces:

$$-K\frac{\partial T}{\partial x_i} = h.\Delta T \tag{16}$$

where ΔT, $T_{mold} - T_\infty$ at the mold/cooling water interface;

T_{mold} is the mold temperature;

$\Delta T = T_{metal} - T_{mold}$ at the metal/mold interface.

Using Eq. (16) for the case of mold/cooling water interface, Eq. (16) can be regrouped as:

$$-K\frac{\partial T_{mold}}{\partial x_i} = h(T_{mold} - T_\infty) \tag{17}$$

Integration of Eq. (17) in space gives:

$$T_{mold} = T_\infty + (T_{mw} - T_\infty)e^{-\frac{h}{K}(x_i - x_{mw})} \tag{18}$$

where T_{mw}, temperature at the mold wall [K];

x_{mw}, position at the mold wall [m].

Thus, when x has the value of the x-coordinate at the interface (wall), temperature T becomes temperature of the interface (wall). Taking the second derivative of this expression with respect to x-coordinate and substitute in the fundamental equation of heat conduction, the result will be

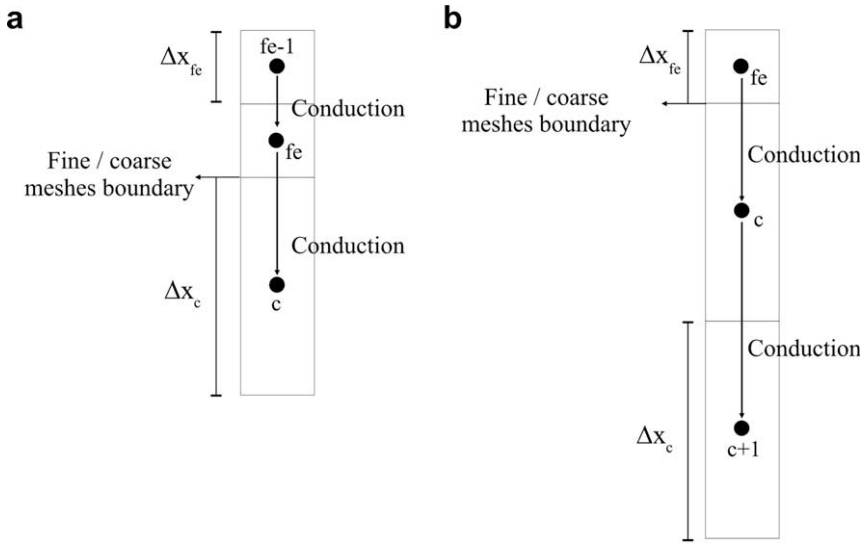

Fig. 6. Schematic representation of fine/coarse meshes connection (a) heat balance for the 'fe' (fine) element (b) heat balance for the 'c' (coarse) element.

$$\rho c\frac{dT_{mw}}{dt}=K(T_{mw}-T_{\infty})\frac{h^2}{K^2}e^{-\frac{h}{K}(x_i-x_{mw})} \tag{19}$$

After regrouping Eq. (19) becomes:

$$dT_{mw}=\frac{h^2}{(\rho cK)_{mold}}(T_{mw}-T_{\infty})e^{-\frac{h}{K}(x_i-x_{mw})}dt \tag{20}$$

Integrating Eq. (20) at the wall in time and assuming that "h" is explicitly constant in time:

$$\ln\left(\frac{T_{mw}-T_{\infty}}{T_{mwt=0}-T_{\infty}}\right)=\frac{h^2}{(\rho cK)_{mold}}t \tag{21}$$

Isolating "h", it gives:

$$h=\left[(\rho cK)_{mold}\ln\left(\frac{T_{mw}-T_{\infty}}{T_{mwt=0}-T_{\infty}}\right)\right]^{\frac{1}{2}}t^{-\frac{1}{2}} \tag{22}$$

where $T_{mwt=0}$ = initial temperature at the mold wall.

Similarly, for the case of the metal/mold interface an expression can be determined:

Eqs. (21) and (22) suggests "h" profile equation in the following form:

$$h=at^{-m} \tag{23}$$

where a and m are constants.

Similarly, using Eq. (20) as the model for "h", for the metal/mold interface:

$$\frac{dT_{mew}}{T_{mew}-T_{mw}}=\frac{a^2t^{-2m}}{(\rho cK)_{metal}}e^{-\frac{at^{-m}}{K}(x_i-x_{mew})}dt \tag{24}$$

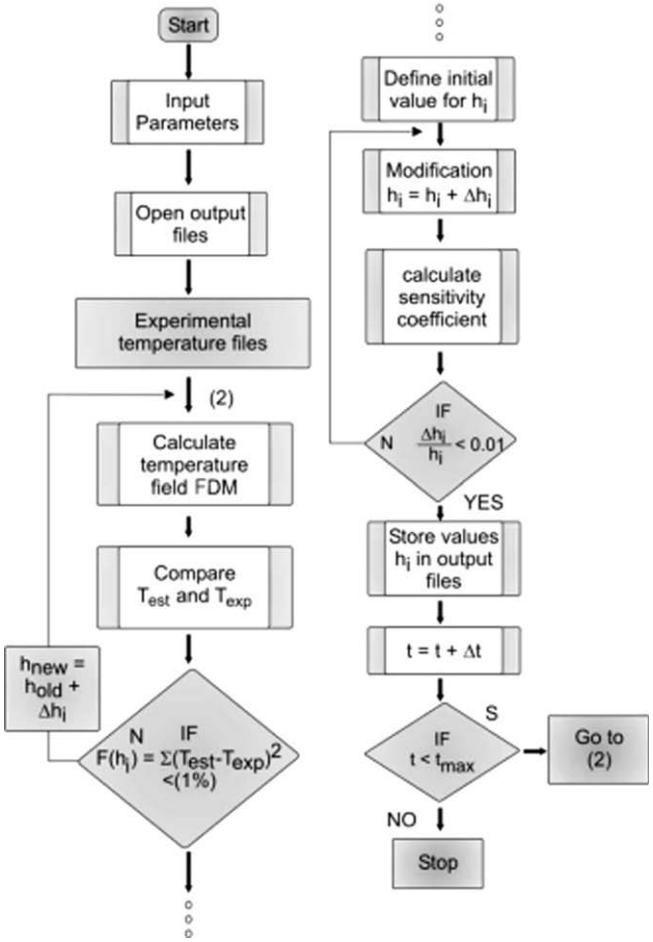

Fig. 7. Flow chart for the determination of transient metal/coolant heat transfer coefficient.

x_{mew}, position at the ingot wall [m].

At the solid/melt interface ($x = x_{mew}$):

$$\frac{dT_{mew}}{T_{mew}-T_{mw}}=\frac{a^2t^{-2m}}{(\rho cK)_{metal}}dt \tag{25}$$

Integrating Eq. (25):

$$\ln\left(\frac{T_{mew}-T_{mw}}{T_{mewt=0}-T_{mw}}\right)=\frac{a^2}{(-2m+1)(\rho cK)_{metal}}t^{-2m+1} \tag{26}$$

Hence, the temperature of the ingot wall will vary in time as:

$$T_{mew}=T_{mw}+(T_{mewt=0}-T_{mw})e^{\frac{a^2}{(-2m+1)(\rho cK)_{metal}}t^{-2m+1}} \tag{27}$$

If $T_{mew\ t=0} > T_{mw}$ and $m < 0.5$, the temperature of the ingot wall will decrease from its initial value down to the temperature of the mold wall (as time goes to infinity). However, if $T_{mew\ t=0} > T_{mw}$ and $m > 0.5$, the temperature of the ingot wall will not equal its initial temperature even when time is $t = 0$.This suggests that only values $m < 0.5$ are acceptable. By analyzing previous studies concerning the evaluation of metal/mold heat transfer coefficients for a number of metallic alloys [12,15,16] it can be seen that the restriction $m < 0.5$ complies with all the resulting experimental equations.

Since the temperature difference at the interface is unknown, an inverse heat transfer technique was used to estimate interfacial heat transfer rates. This can be accomplished by using the temperature history furnished by each thermocouple. The method used to determine the transient metal/coolant heat transfer coefficient, h, is based on the solution of the Inverse Heat Conduction Problem

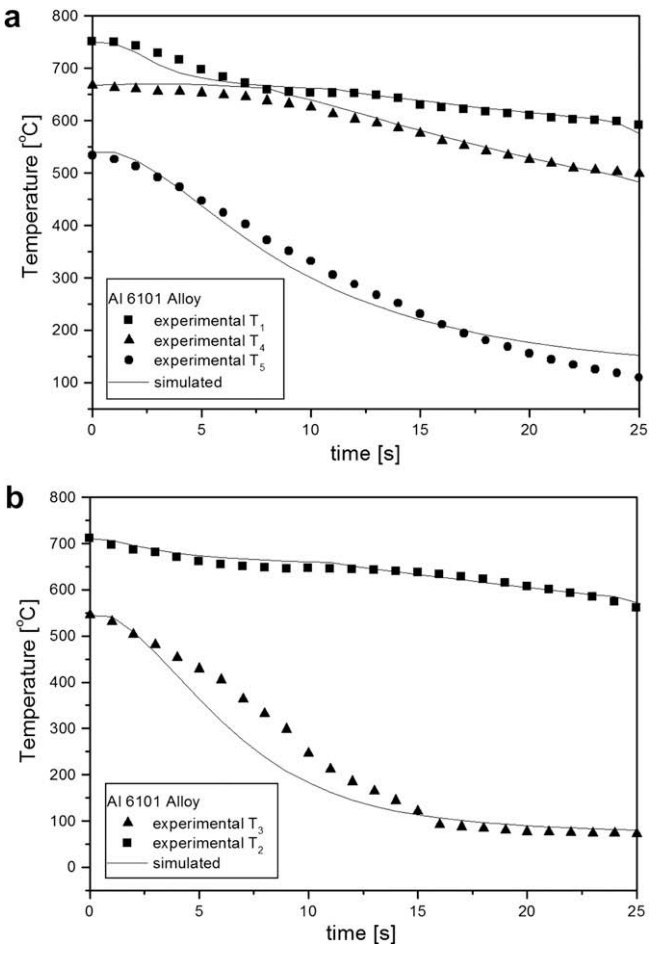

Fig. 8. Experimental and simulated temperatures. Al 6101 alloy (a) positions T_1 (ingot top), T_4 (ingot bottom) and T_5 (mold bottom) (b) positions T_2 (ingot lateral) and T_3 (mold lateral).

(IHCP) [22]. This method makes a complete mathematical description of the physics of the process and is supported by temperature measurements at known locations inside the heat conducting body. The temperature files containing the experimentally monitored temperatures are used in a finite difference heat flow model to determine h. The process at each time step included the following: a suitable initial value of h is assumed and with this value, the temperature of each reference location in casting and in mold at the end of each time interval Δt is simulated by the numerical model. The correction in h at each interaction step is made by a value Δh, and new temperatures are estimated $[T_{est}(h+\Delta h)]$ or $[T_{est}(h-\Delta h)]$. With these values, sensitivity coefficients (Φ) are calculated for each interaction, given by:

$$\Phi = \frac{T_{est}(h+0.5\Delta h) - T_{est}(h-0.5\Delta h)}{\Delta h} \quad (28)$$

The procedure determines the value of h, which minimizes an objective function defined by:

$$F(h) = \sum_{i=1}^{n} (T_{est} - T_{exp})^2 \quad (29)$$

where T_{est} and T_{exp} are the estimated and the experimentally measured temperatures at various thermocouples locations and times, and n is the iteration stage. The steps adopted in the determination of h are depicted in the flowchart of Fig. 7. The applied method is a simulation assisted one and has been used in recent publications for determining h for a number of solidification situations [12,15,16,23].

4. Results and discussion

Fig. 8 shows the comparison between experimental thermal responses and those which resulted from individual numerical simulations for each corresponding thermocouple position inside metal and mold. The level of errors in the predicted values of h (Fig. 8) could be potentially significantly reduced by minimizing the L2 norm given in Eq. (29) with the help of a robust hybrid optimization algorithm [24] capable of fast convergence while avoiding local minima.

Table 2 shows the resulting equations describing the metal/mold transient heat transfer coefficients (h), at characteristic interfaces along the ingot cross section. They express h [W.m^{-2}.K^{-1}] as a power function of time, as shown by Eq. (23). It can be observed that all values of "m" are below 0.5.

The infinite value of heat flux at time 0 simultaneously implies a heat transfer coefficient going to infinity. Mathematically, it is evident that this infinite value should only apply to very limited physical situations. With the evolution of solidification, the metal's contraction phenomenon, the physical and chemical characteristics of both metal and mold, and mold expansion during solidification, are mechanisms, which are responsible for the air gap formation at the metal/mold interface. In other words, the main factors which govern the heat flux profile deviation from the perfect thermal contact condition are: liquid metal/mold surface wetability, shrinkage and air gap formation. These factors retard the interfacial heat transfer from the solidifying metal to the mold. The decay tendency of Eq. (23) is a form to relate 'h' to such factors [16].

It can be noticed that the same expression is applied equally for the ingot/lateral mold and for the ingot/stainless steel band interfaces. Due to the relatively high volumetric and thermal contraction of Al alloys along solidification, the ingot gradually detaches from the mold sides and the ingot weight favors the thermal contact between metal and mold at the bottom. Such behavior is reflected by the corresponding h_{bottom} profile, representing the best metal/mold interfacial heat transfer efficiency, as shown in Table 2. It can also be seen that the h_{water} profile has an inverse behavior if compared to those commented before and characterized by Eq. (23). At the beginning of the experiment, given that the mold was previously heated, the water quickly transforms into vapor hindering the heat exchange. When the vapor generation starts to be suppressed, the heat extraction becomes more effective.

Once determined the cooling conditions, reflected by the different h profiles, a direct linear relation can be established between liquid pool length and solid shell evolution with the rotary speed. As a first approach for simulations, the different metal/mold boundary conditions will be considered in calculations by assuming that the transient h_{up}, $h_{lateral}$, and h_{bottom} are connected with the same metal/mold interface along the entire rotary drum. In other words, h_{up} is connected to the outer heat transfer surface,

Table 2
Transient heat transfer coefficients

h [W.m^{-2}.K^{-1}]	Al 6101
h_{bottom}	11000 $t^{-0.01}$
h_{up}	3000 $t^{-0.01}$
$h_{lateral}$	3000 $t^{-0.01}$
h_{water}	5000 $t^{0.8}$

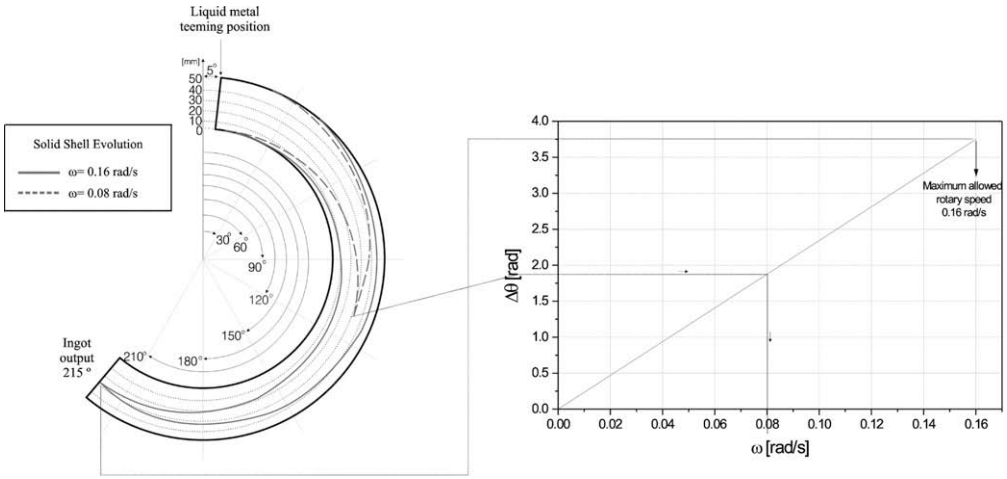

Fig. 9. Solid shell evolution related to the rotary speed according to the determined interfacial cooling conditions.

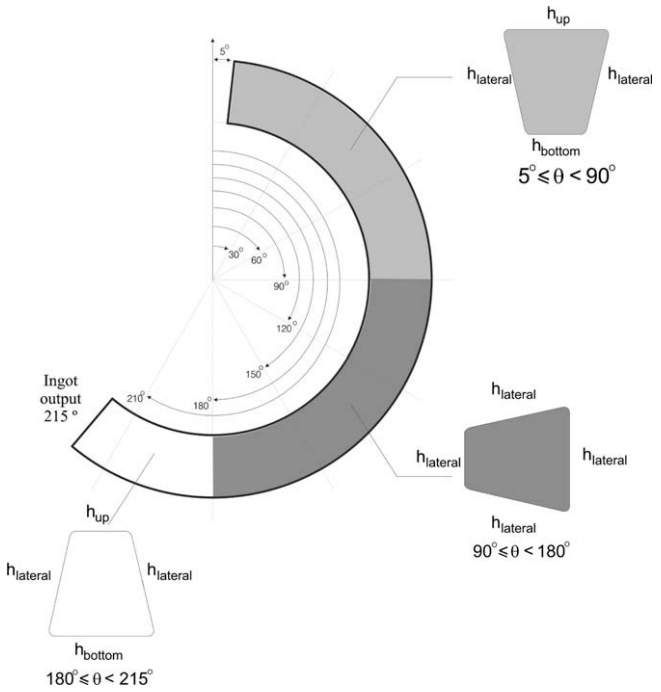

Fig. 10. Approach adopted in numerical simulations to take into account the variable metal/mold boundary conditions along the rotary caster.

h_{bottom} is connected to the inner surface and so on, i.e., the variation of thermal interfacial conditions with the rotary action (and consequently with the gravity orientation) will not be taken into account. The simulated results are shown in Fig. 9. In terms of production optimization, the maximum allowed rotary speed for the Al 6101 alloy was shown to be 0.16 rad/s, which guarantees the complete solidification at the ingot output.

In industrial rotary casters the ingot experiences a change on the metal/mold boundary conditions along the solidification process. At the pouring region, the higher interfacial heat transfer efficiency at the mold bottom (characterized by h_{bottom}) is due to the gravitational effect. Such efficiency decreases gradually along the caster and at a position $\theta = 90°$, the boundary condition h_{bottom} is replaced by $h_{lateral}$ and at a position $\theta = 180°$, when the ingot enters a near horizontal orientation normal to the gravity vector, h_{bottom} is replaced by h_{up}, as depicted in Fig. 10. The other boundary conditions connected to the different metal/mold surfaces are equally influenced by the rotating action, with each boundary condition being affected by the radial position. Any accurate numerical analysis of solidification along the rotary caster must ultimately confront the complexity of such boundary conditions. In the present analysis an approach is proposed which, for numerical simulations purposes, divide the circumference of the drum from the pouring point ($\theta = 5°$) up to the ingot output ($\theta = 215°$) into three different zones which are characterized by different $h = f(t)$ functions, as shown in Fig. 10. The simulated results based on such approach are shown in Fig. 11. With the adoption of such variation on h, the ingot took about 3 seconds more to completely solidify if compared to the previous simulation condition shown in Fig. 9. As a result of this solidification time delay, the maximum allowed rotary speed has decreased to 0.14 rad/s. Another comparison can be made concerning the point of complete solidification. Fig. 9 shows that such point is out of the ingot geometrical center whilst in the last approach (Fig. 11), the simulation has shown that the complete solidification occurs exactly at the geometric center of the casting.

5. Conclusions

Experiments were carried out to analyze the behavior of metal-mold and mold-water heat transfer coefficients (h) during solidification of an aluminum alloy in a simulator which uses a sector of a Properzi rotary industrial caster. The following conclusions can be drawn:

– The transient interfacial heat transfer coefficient (h) has been characterized by using a technique based on measured temperatures along casting and chill, and numerical simulations provided by a numerical heat transfer model based on an IHCP procedure. The metal–mold heat transfer coefficients have been expressed as a power function of time (t), by:

$$h = at^{-m}$$

where a and m are constants, and $m < 0.5$.

–The resulting equations for h have shown that the metal/mold heat transfer efficiency is similar at the ingot sides and top. In contrast, the gravitational effect induces much better interfacial heat transfer efficiency at the ingot bottom, of about three times higher than that exhibited at the ingot sides and top.

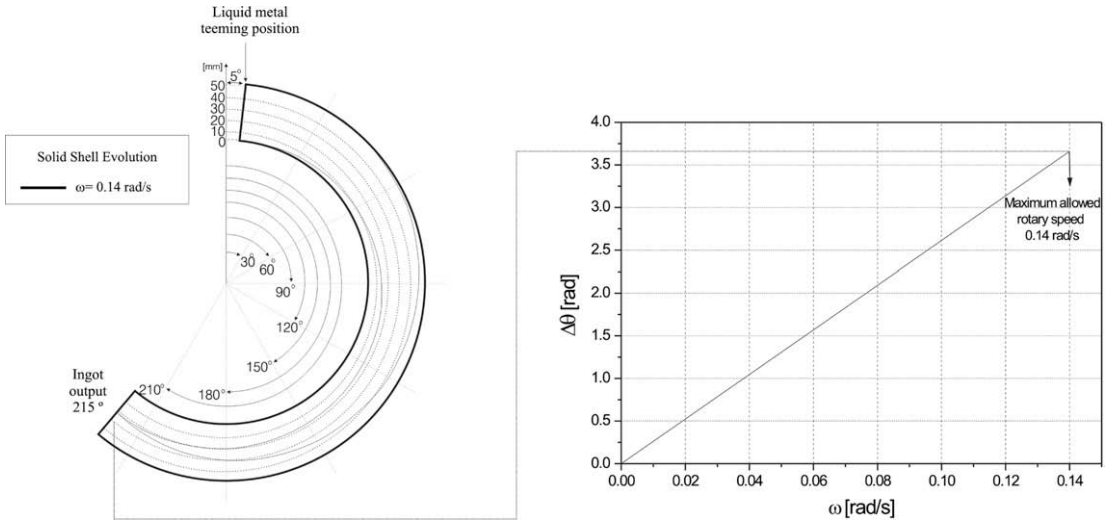

Fig. 11. Solid shell evolution related to rotary speed according to the variable interfacial cooling conditions approach proposed in Fig. 10.

–The use of an approach based on variable $h = f(t)$ functions for each metal/mold surface along the rotating drum has permitted a more accurate representation of the solidification evolution along the rotary casting to be determined.
–The determination of heat transfer coefficients along the different metal/mold interfaces has permitted the optimization of the rotary speed with a view to increase ingot industrial production.

Acknowledgements

The authors acknowledge financial support provided by FAPESP (The Scientific Research Foundation of the State of São Paulo, Brazil) FAEPEX–UNICAMP, CNPq (The Brazilian Research Council) and ALUBAR.

References

[1] R.D. Pehlke, in: Metals Handbook, vol. 15, ASM International, Materials Park, Ohio, 1988, pp. 308–316.
[2] Ch. Gras, M. Meredith, J.D. Hunt, Microstructure and texture evolution after twin roll casting and subsequent cold rolling of Al–Mg–Mn aluminium alloys, Journal of Materials Processing Technology 169 (2005) 156–163.
[3] J.E. Spinelli, J.P. Tosetti, C.A. Santos, J.A. Spim, A. Garcia, Microstructure and solidification thermal parameters in thin strip continuous casting of a stainless steel, Journal of Materials Processing Technology 150 (2004) 255–262.
[4] A.G. Gerber, A.C.M. Sousa, Numerical investigation of the influence of air gaps upon the solidification in a rotary caster, Journal of Materials Processing Technology 48 (1995) 657–665.
[5] Y. Meng, B.G. Thomas, Heat-transfer and solidification model of continuous slab casting: CON1D, Metallurgical and Materials Transactions B: Process Metallurgy and Materials Processing Science 34B (2003) 685–705.
[6] C.A. Santos, J.A. Spim, A. Garcia, Mathematical modeling and optimization strategies (genetic algorithm and knowledge base) applied to the continuous casting of steel, Engineering Applications of Artificial Intelligence 16 (2003) 511–527.
[7] N. Cheung, A. Garcia, Use of a heuristic search technique for the optimization of quality of steel billets produced by continuous casting, Engineering Applications of Artificial Intelligence 14 (2001) 229–238.
[8] C.A. Santos, E.L. Fortaleza, C.R. Ferreira, J.A. Spim, A. Garcia, A solidification heat transfer model and a neural network based algorithm applied to the continuous casting of steel billets and blooms, Modelling and Simulation in Materials Science and Engineering 13 (2005) 1071–1087.
[9] N. Cheung, C.A. Santos, J.A. Spim, A. Garcia, Application of a heuristic search technique for the improvement of spray zones cooling conditions in continuously cast steel billets, Applied Mathematical Modelling 30 (2006) 104–115.
[10] Z. Guo, N. Saunders, A.P. Miodownik, J.Ph. Schillé, Modelling of materials properties and behaviour critical to casting simulation, Materials Science and Engineering A 413/414 (2005) 465–469.
[11] X.K. Lan, J.M. Khodadadi, Liquid steel flow, heat transfer and solidification in mold of continuous casters during grade transition, International Journal of Heat and Mass Transfer 44 (2001) 3431–3442.
[12] I.L. Ferreira, J.E. Spinelli, J.C. Pires, A. Garcia, The effect of melt temperature profile on the transient metal/mold heat transfer coefficient during solidification, Materials Science and Engineering A 408 (2005) 317–325.
[13] W.D. Griffiths, A model of the interfacial heat-transfer coefficient during unidirectional solidification of an aluminum alloy, Metallurgical and Materials Transactions B: Process Metallurgy and Materials Processing Science 31B (2000) 285–295.
[14] J.A. Hines, Determination of interfacial heat transfer boundary conditions in an aluminum low pressure permanent mold test casting, Metallurgical and Materials Transactions B: Process Metallurgy and Materials Processing Science 35B (2004) 299–311.
[15] J.E. Spinelli, I.L. Ferreira, A. Garcia, Evaluation of heat transfer coefficients during upward and downward transient directional solidification of Al–Si alloys, Structural and Multidisciplinary Optimization 31 (2006) 241–248.
[16] E.N. Souza, N. Cheung, C.A. Santos, A. Garcia, The variation of the metal/mold heat transfer coefficient along the cross section of cylindrical shaped, Inverse Problems in Science and Engineering 14 (2006) 467–481.
[17] M.A. Martorano, J.D.T. Capocchi, Heat transfer coefficient at the metal–mould interface in the unidirectional solidification of Cu-8%Sn alloys, International Journal of Heat and Mass Transfer 43 (2000) 2541–2552.
[18] W. Wang, H.H. Qiu, Interfacial thermal conductance in rapid contact solidification process, International Journal of Heat and Mass Transfer 45 (2002) 2043–2053.
[19] D.J. Browne, D. O'Mahoney, Interface heat transfer in investment casting of aluminum alloys, Metallurgical and Materials Transactions A: Physical Metallurgy and Materials Science 32 (2001) 3055–3063.
[20] F.P. Incropera, D.P. Dewitt, Fundamentals of Heat and Mass Transfer, third ed., John Wiley & Sons, New York, 1990.
[21] R.W. Ruddle, The Solidification of Castings, Institute of Metals, London, 1957.
[22] J.V. Beck, Nonlinear estimation applied to the nonlinear inverse heat conduction problem, International Communications in Heat and Mass Transfer 13 (1970) 703–716.
[23] M. Krishnan, D.G.R. Sharma, Determination of the interfacial heat transfer coefficient h in unidirectional heat flow by Beck's non linear estimation procedure, International Communications in Heat and Mass Transfer 23 (1996) 203–214.
[24] M.J. Colaco, H.R.B. Orlande, G.S. Dulikravich, Inverse and optimization problems in heat transfer, Journal of the Brazilian Society of Mechanical Science & Engineering 28 (2006) 1–23.